

## Rotating Field Confinement of Pure Electron Plasmas Using Trivelpiece-Gould Modes

F. Anderegg, E. M. Hollmann, and C. F. Driscoll

*Institute for Pure and Applied Physical Sciences and Department of Physics, University of California at San Diego,  
La Jolla, California 92093*

(Received 13 August 1998)

A “rotating wall” electric field is shown to give steady-state confinement of a column of  $3 \times 10^9$  electrons in a Penning-Malmberg trap at 4 tesla. By increasing the frequency of the rotating drive, a central-density compression by a factor of 20 has been obtained. For both dipole and quadrupole drives (i.e.,  $m_\theta = 1$  and 2), the compression rate depends on drive frequency, exhibiting peaks associated with  $k_z \neq 0$  Trivelpiece-Gould plasma modes. The drive also causes plasma heating, but cyclotron radiation cooling keeps the temperature low enough that background gas ionization is negligible. [S0031-9007(98)07771-0]

PACS numbers: 52.25.Wz, 52.25.Fi

Non-neutral electron or ion plasmas confined in Penning-Malmberg traps have inherent confinement times which are long, but finite. In practice, background neutral gas and small confinement field asymmetries exert a drag on the rotating plasma, causing slow radial expansion and eventual particle loss. Previous work [1] on small ion plasmas has demonstrated radial compression and steady-state confinement using laser techniques to apply a torque which counteracts the drag on the plasma. However, there is considerable interest in containment of elementary particles, including antimatter [2], where laser techniques are not applicable.

Recently, “rotating wall” electric fields applied to the end of a column of  $10^9$   $\text{Mg}^+$  ions have been shown to give steady-state confinement and compression up to 20% of the Brillouin density limit [3]. The  $\mathbf{E} \times \mathbf{B}$  rotation rate  $f_E$  of the ions is observed to be somewhat less than the wall rotation frequency  $f_w$ , with a “slip” frequency  $\Delta f \equiv f_E - f_w$  varying with ion temperature as  $\Delta f \propto T^{1/2}$ . The rotating wall technique has also been applied to spheroidal ion plasmas in the strongly correlated or crystalline regimes [4]; here, the applied perturbation was axially uniform along the plasma, and the plasma rotation was generally observed to be phase locked to the rotating field (i.e.,  $\Delta f = 0$ ).

Previously, modest density and angular momentum changes of electron columns were reported [5] when an applied dipolar perturbation excited a plasma mode, but strong plasma heating limited the technique at low magnetic fields. Other experiments [6] utilize this heating to replenish the electron plasma by ionization.

In this Letter, we describe pure electron plasmas confined by rotating dipole ( $m_\theta = 1$ ) and quadrupole ( $m_\theta = 2$ ) electric fields applied at one end of the plasma column. We show that the torque can be used to control and compress the plasma. The torque is shown to arise from Trivelpiece-Gould (TG) plasma modes with axial wave numbers  $k_z \neq 0$  whose frequencies determine the nonzero slip  $\Delta f$ . The rotating wall generates some plasma heating, but here cyclotron radiation cooling keeps

the plasma temperature low, so background gas ionization is negligible.

Figure 1 shows the “IV” Penning-Malmberg trap consisting of cylindrical electrodes in ultrahigh vacuum ( $P \approx 3 \times 10^{-9}$  Torr, 97%  $\text{H}_2$ ), in a uniform axial magnetic field ( $B = -4 \text{ T } \hat{z}$ ). This apparatus normally contains  $\text{Mg}^+$  ions continuously diagnosed by laser-induced fluorescence [7]; here, we contain only electrons and operate in a standard inject/hold/dump-and-measure cycle [8]. Injection gives a plasma of  $N_{\text{tot}} \approx 3 \times 10^9$  electrons in a column of length  $L_p \approx 35$  cm, radius  $R_p \approx 0.27$  cm, and central density  $n_0 \approx 4.5 \times 10^8 \text{ cm}^{-3}$ , bounded by the cylindrical walls at  $R_w = 2.86$  cm. Axial confinement is assured by negative voltages applied to the end electrodes, and radial confinement is provided by the magnetic field.

The plasma density profile  $n(r)$  and an estimate of the thermal energy  $T$  are obtained by dumping the plasma axially and measuring the charge passing through a hole in a scanning collimator plate. Both measurements require shot-to-shot reproducibility of the injected plasma, and we typically obtain variability  $\delta n/n \lesssim 1\%$ . Figure 2 shows the radial density profile ( $I$ ) for the initial plasma 5 sec after injection, and profiles after plasma expansion ( $E$ ) or compression ( $C$ ) as described below. The temperature  $T$  characterizing the parallel energy

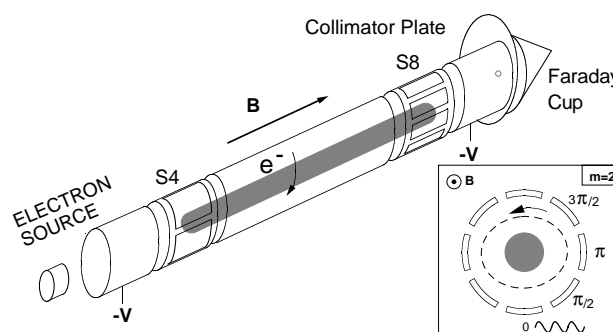


FIG. 1. Schematic diagram of the cylindrical ion trap, with inset representing the rotating wall drive on sectored cylinder S8.

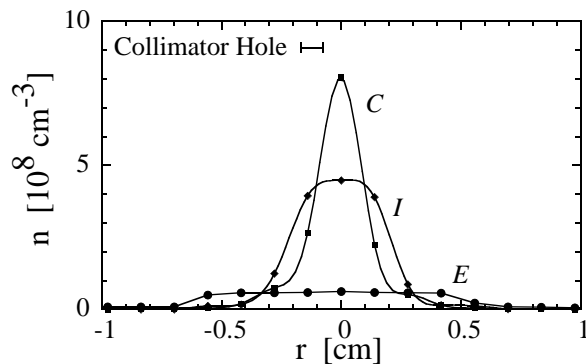


FIG. 2. Radial electron density profiles for the injected plasma (I), a compressed plasma (C), and an expanded plasma (E).

distribution is obtained by slowly dumping the center of the plasma and measuring charge versus confinement voltage [9]. Here, we presume that  $T_{\parallel} = T_{\perp} \equiv T$ , since the collision rate  $\nu_{\perp\parallel} \equiv (8/15)\sqrt{\pi}nb^2\bar{v} \ln \Lambda \approx (1050 \text{ sec}^{-1})(T/1 \text{ eV})^{-3/2}(n/10^8 \text{ cm}^{-3})$  is relatively rapid.

The radial expansion or compression of the plasma is determined by changes in the total angular momentum  $P_{\theta}$ , given by  $P_{\theta} \equiv \sum_j [mv_{\theta j}r_j - eBr_j^2/2c] \approx -(eB/2c)\sum_j r_j^2$ , with the sum over the  $N_{\text{tot}}$  particles. At low temperature and low density, the angular momentum in the electromagnetic field dominates, so conservation of angular momentum implies conservation of the mean-square radius of the plasma. In practice, inherent “background” asymmetries [10] exert a weak drag on the rotating plasma, causing a decrease in  $P_{\theta}$  and a bulk expansion of the plasma. Measurements show that this “mobility” expansion rate scales roughly as  $\tau_m^{-1} \equiv -(\dot{n}_0/n_0)_{\text{bkg}} \approx (7 \times 10^{-4} \text{ sec}^{-1})(n_0/10^8 \text{ cm}^{-3})^2$  for the electron columns studied here. To maintain or compress the plasma, the rotating wall drive must supply a positive torque as large or larger than this drag; alternately, a reverse-rotating drive can substantially increase the background expansion rate.

One practical way to compress the plasma is to ramp the rotating wall drive from low frequency to high frequency; Fig. 3 shows the density compression and heating which result from ramped  $m_{\theta} = 1$  and  $m_{\theta} = 2$  drives. The drive consists of sinusoidal voltages  $\Phi_{w j} = A_w \cos(m_{\theta}\theta_j - 2\pi f_s t)$  applied to the eight sectors at  $\theta_j = 2\pi j/8$ . Here,  $f_s = m_{\theta}f_w$  is the signal generator frequency. In Fig. 3a, the  $m_{\theta} = 1$  drive frequency is ramped linearly from 0.5 to 2.13 MHz in 1000 sec, starting with the injected profile I. Initially, while  $0.5 < f_s < 0.7$  MHz, the central density slowly decreases, indicating that there is no significant positive torque from the wall drive. Then, when  $0.7 < f_s < 2.0$  MHz, the plasma density increases (and the plasma radius decreases), maintaining equilibrium with the drive. When  $f_s > 2.0$  MHz, the density rapidly decreases a factor of 2 until eventually a

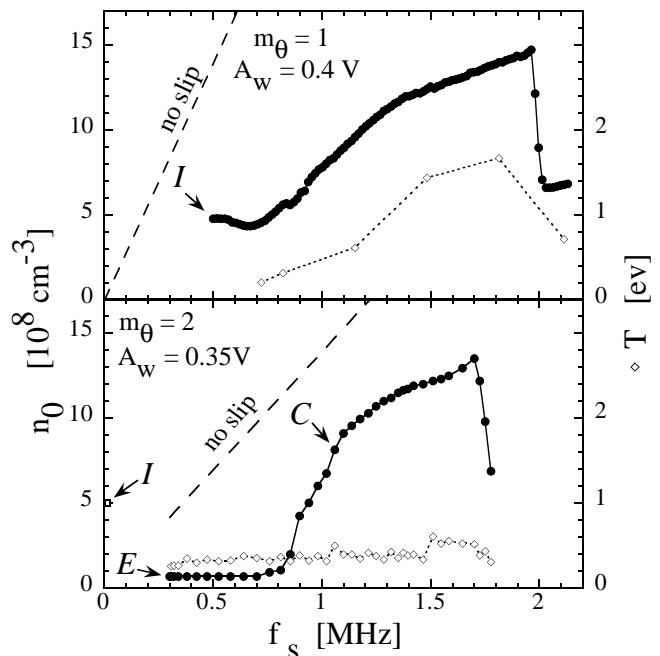


FIG. 3. Central density versus ramped rotating drive frequency  $f_s$  for  $m_{\theta} = 1$  and 2, and measured temperatures during the ramp.

different torque-balanced equilibrium is reached; below, this will be interpreted as locking to a different TG mode.

Density compression by a factor of 20 from an  $m_{\theta} = 2$  drive is shown in Fig. 3b; here the ramped drive frequency was applied to an initially expanded plasma with profile E of Fig. 2. This expanded plasma was obtained from the injected profile I by applying a *reverse-rotating*  $m_{\theta} = 2$  perturbation at  $-1.0$  MHz for 50 sec; the forward drive was then ramped from 0.3 to 1.8 MHz in 415 sec. For  $0.3 < f_s < 0.8$  MHz, no compression was observed. For  $0.8 < f_s < 1.7$  MHz, a torque-balanced equilibrium was obtained, where the central density increased with the ramp frequency. Profile C of Fig. 2 was taken after ramping to 1.05 MHz. For  $1.7 < f_s < 1.8$  MHz, the background drag at high density was larger than the applied torque, and no equilibrium was obtained before the process was terminated.

In these compressions, the central plasma density always remains well below the “no slip” density defined by  $f_E = f_w$ , where  $f_E \equiv cen_0/B$  is the central  $\mathbf{E} \times \mathbf{B}$  rotation frequency. One might more properly consider the fluid rotation frequency  $f_R(r)$ , but here  $f_R \approx f_E$  since the diamagnetic and centrifugal drift terms are small. Thermodynamics arguments [11] suggest that one must have  $f_R \leq f_w$  to obtain a positive torque.

The plasma temperature is substantially increased by the rotating wall drive. When undriven, the trapped electron column typically relaxes to  $T \approx 0.1\text{--}0.2$  eV, at which point cooling and heating affects balance. Cooling is provided by cyclotron radiation [12], with  $-\dot{T}/T \equiv \tau_c^{-1} = (4 \text{ sec}^{-1})(B/4T)^2$ , and electron-neutral collisions

may also cool the plasma. Heating results when plasma expansion liberates the electrostatic energy, with  $\dot{T} \approx e\varphi_p/\tau_m$ , where  $\varphi_p$  is the central plasma potential. The rotating wall drive contributes additional heating through the excitation and damping of plasma waves. The heating appears to be greater for  $m_\theta = 1$  than for  $m_\theta = 2$ , perhaps because  $f_w = f_s/m_\theta$  is greater.

We find that the applied drive couples to the plasma through discrete finite-length TG plasma mode resonances [13]. Figure 4 shows the resulting peaks in the initial compression rate versus drive frequency when a *small amplitude* drive is applied to a plasma with profile *I* of Fig. 2. Here, an  $m_\theta = 1$  rotating drive at a chosen frequency is applied to S8, and the initial central compression (or expansion) rate  $\dot{n}_0/n_0$  is measured. The measured background expansion rate of  $(\dot{n}_0/n_0)_{\text{bkg}} = -3 \times 10^{-3} \text{ sec}^{-1}$  has been subtracted from the data, so the plot indicates torque from the rotating drive alone. In addition, we measure the wave power at frequency  $f_s$  received on S4 at the other end of the plasma. Distinct peaks in the compression rate are observed, and distinct (10–30 dB) wave transmission peaks are observed at the frequencies marked by down arrows.

The six observed wave transmission peaks correspond closely with the numerical drift-kinetic predictions for TG plasma modes varying as  $\exp(im_\theta\theta + im_z z\pi/L_p)$  and having  $m_r$  zeros in the radial eigenfunction (counting the one at  $r = 0$ ). The TG modes for long columns within a cylindrical wall [13] have a rotationally shifted “acoustic” dispersion relation, given approximately by

$$f - m_\theta f_E \approx \pm g(m_r, T) \frac{\omega_p}{2\pi} R_p \frac{\pi m_z}{L_p}. \quad (1)$$

The shifted frequencies are proportional to  $N_{\text{tot}}^{1/2}$  through  $\omega_p \equiv (4\pi ne^2/m)^{1/2}$  and  $R_p$ , are proportional to  $k_z \equiv \pi m_z/L_p$ , and depend functionally on  $T$  and  $m_r$ . In contrast, the radial density profile  $n(r)$  and absolute column

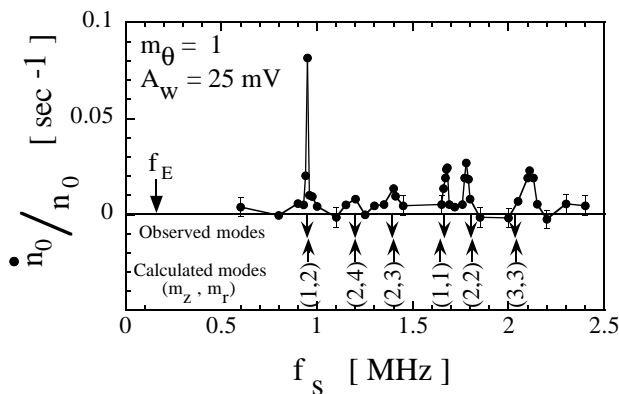


FIG. 4. Density compression rates versus rotating drive frequency for a small amplitude drive,  $m_\theta = 1$ , compared to the observed and calculated Trivelpiece-Gould plasma mode frequencies for various  $(m_z, m_r)$ . The temperature remains low, with  $T \lesssim 0.2$  eV.

size  $R_p$  have little effect on the mode frequencies except through  $m_\theta f_E$ . The predicted frequencies for the  $m_\theta = 1$  and the lowest  $(m_z, m_r)$  modes are shown by the up arrows in Fig. 4. For a plasma of  $N_{\text{tot}} = 3 \pm 0.6 \times 10^9$  and  $L_p = 35$  cm, this small amplitude ( $A_w = 25$  mV) drive does not measurably heat the plasma, so  $T \approx 0.1$ – $0.2$  eV. The predicted modes agree quantitatively with the six wave transmission peaks and with the six compression peaks once the particle number and temperature were adjusted to  $N_{\text{tot}} = 2.7 \times 10^9$  and  $T = 0.1$  eV. This correspondence has been further verified by varying the plasma length and by tailoring the antenna configuration to distinguish even and odd  $m_z$ .

Figure 5 shows that a *large amplitude* rotational drive causes broad, nonlinear compression and heating peaks in addition to general heating. Here, the 0.4 V drive at  $f_s$  was applied to profile *I*, and the initial compression and heating rates were measured. This heating causes large shifts in the compression peaks. For example, the numerical mode calculation shows that the  $m_\theta = 1, (1,2)$  mode varies as

$$f_{(1,2)}^{(1)}(T) \approx 0.79 + 0.75T^{0.5} \text{ [MHz]}. \quad (2)$$

This predicted frequency shift is verified by small amplitude wave transmission experiments with controlled heating from 0.2 to 0.5 eV. Also we note that negative torque peaks and heating peaks are clearly observed for the reverse drive direction with  $m_\theta = 1$ ; for  $m_\theta = 2$ , the negative peaks were substantially smaller and less “reproducible” in practice.

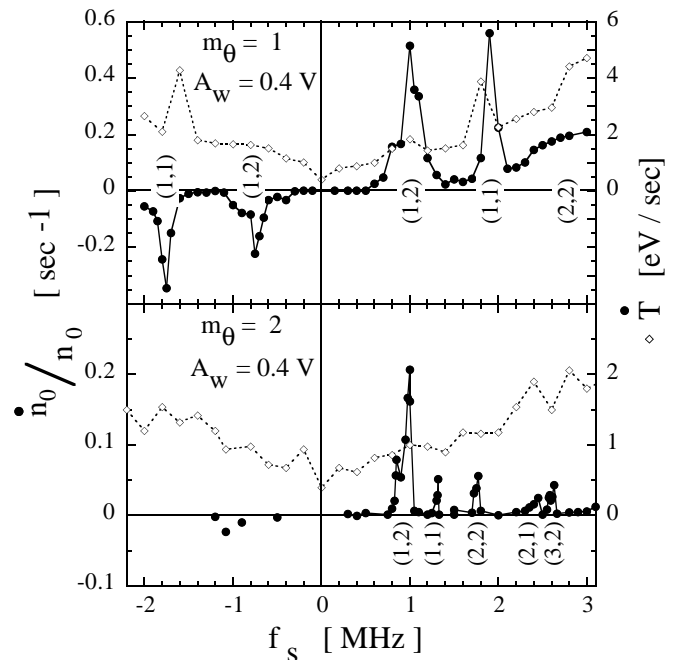


FIG. 5. Density compression rates and plasma heating for large amplitude  $m_\theta = 1$  and  $m_\theta = 2$  rotating drives. The compression peaks are associated with shifted  $(m_z, m_r)$  modes.

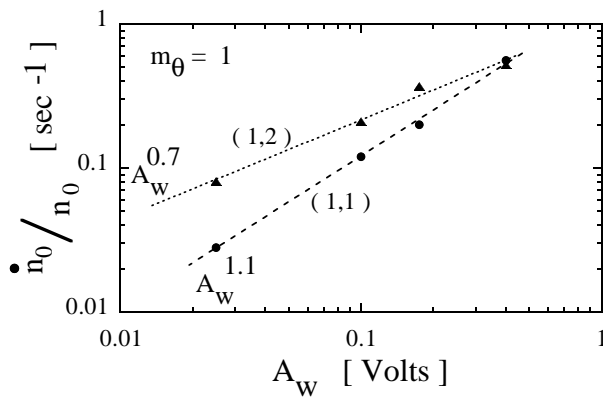


FIG. 6. Peak density compression rates versus amplitude for the two prominent  $m_\theta = 1$  modes.

The measured compression peaks of Fig. 5 explain the characteristics of the density ramps of Fig. 3. For  $m_\theta = 1$ , the (1,2) peak gives significant positive torque only for  $f_s > 0.6$  MHz, at which point the central density begins to ramp up. As  $f_s$  is increased, the torque-balance equilibrium “rides up” the left side of the (1,2) peak. As the plasma is compressed,  $f_E$  increases, and the mode frequency increases. For the maximally compressed plasma with  $n_0 = 14.5 \times 10^8 \text{ cm}^{-3}$ , we measure the (1,2) compression peak to give  $(\dot{n}_0/n_0)_{\text{rw}} \approx 0.1 \text{ sec}^{-1}$  and the background free expansion rate to be  $(\dot{n}_0/n_0)_{\text{bkg}} \approx -0.11 \text{ sec}^{-1}$ ; this peak compression is less than in Fig. 5, presumably because the column is radially compressed. For  $f_s > 2.0$  MHz, the plasma expands until a new torque-balance equilibrium is obtained on the left side of the (2,2) compression peak, since the (1,1) and (1,2) peaks are merged together for  $T \geq 1 \text{ eV}$ .

The nonlinear nature of the  $m_\theta = 1$  rotating drive is demonstrated in Fig. 6, where the peak compression rates for the (1,1) and (1,2) modes are shown as a function of drive amplitude. The observed scalings of  $A_w^{0.7}$  and  $A_w^{1.1}$  differ markedly from linear theory, which predicts a torque  $\mathcal{T} \propto \dot{n}_0/n_0 \propto \delta n \delta \varphi \propto A_w^2$ , where  $\delta n$  and  $\delta \varphi$  are the density and potential perturbations. Wave transmission experiments suggest that the coupling is more nearly linear below  $A_w = 0.03 \text{ V}$ .

This understanding of torque coupling through TG modes allows a more quantitative understanding of the previous results for ion plasmas [3]. For ions, the  $\omega_p$  term of Eq. (1) is reduced by  $(m_i/m_e)^{1/2}$ , but the  $f_E$  term is independent of mass; this causes the ion modes to appear close together near  $f_E$ . Furthermore, the numerical frequency calculation shows that the ion modes shift substantially with temperature: for example, the  $m_\theta =$

1, (1,2) mode varies as  $f_{(1,2)}^{(1)}(T) \approx 45 + 9.0T^{0.6} \text{ [kHz]}$ . Thus, the previously observed temperature dependence of the ion slip,  $\Delta f \propto T^{1/2}$ , probably arises from TG mode frequency shifts rather than from bounce-resonant particles as previously suggested. Further experiments with ion plasmas are needed to resolve this issue, and to clarify the distinction between the finite-slip  $k_z \neq 0$  couplings described here and the zero-slip  $k_z = 0$  couplings obtained with crystallized ion plasmas [4].

We thank Dr. T.M. O’Neil, Dr. D.H.E. Dubin, Dr. X.-P. Huang, Dr. T.B. Mitchell, Dr. R.E. Pollock, Dr. J.J. Bollinger, and Mr. J. Danielson for stimulating discussions, Dr. R. Spencer for use of his drift-kinetic computer code, and Mr. R. Bongard for construction of a custom 8-channel digital function generator. This work is supported by Office of Naval Research Grant No. N00014-96-1-0239 and National Science Foundation Grant No. PHY94-21318.

- 
- [1] D.J. Heinzen, J.J. Bollinger, F.L. Moore, W.M. Itano, and D.J. Wineland, *Phys. Rev. Lett.* **66**, 2080 (1991).
  - [2] D.S. Hall and G. Gabrielse, *Phys. Rev. Lett.* **77**, 1962 (1996); ATHENA Collaboration, M. Holzscheiter *et al.*, *Hyperfine Interact.* **109**, 1 (1997).
  - [3] X.-P. Huang, F. Anderegg, E.M. Hollmann, C.F. Driscoll, and T.M. O’Neil, *Phys. Rev. Lett.* **78**, 875 (1997).
  - [4] X.-P. Huang, J.J. Bollinger, T.B. Mitchell, and W.M. Itano, *Phys. Rev. Lett.* **80**, 73 (1998).
  - [5] D.L. Eggleston, T.M. O’Neil, and J.H. Malmberg, *Phys. Rev. Lett.* **53**, 982 (1984); T.B. Mitchell, Ph.D. thesis, University of California at San Diego, 1993.
  - [6] R.E. Pollock and F. Anderegg, in *Non-Neutral Plasma Physics II*, edited by J. Fajans and D.H.E. Dubin, AIP Conf. Proc. 331 (AIP, New York, 1994), p. 139.
  - [7] F. Anderegg, X.-P. Huang, E. Sarid, and C.F. Driscoll, *Rev. Sci. Instrum.* **68**, 2367 (1997).
  - [8] J.S. deGrassie and J.H. Malmberg, *Phys. Fluids* **23**, 63 (1980).
  - [9] B.R. Beck, J. Fajans, and J.H. Malmberg, *Phys. Plasmas* **3**, 1250 (1996); D.L. Eggleston, C.F. Driscoll, B.R. Beck, A.W. Hyatt, and J.H. Malmberg, *Phys. Fluids B* **4**, 2432 (1992).
  - [10] C.F. Driscoll, K.S. Fine, and J.H. Malmberg, *Phys. Fluids* **29**, 2015 (1986).
  - [11] T.M. O’Neil and D.H.E. Dubin, *Phys. Plasmas* **5**, 2163 (1998).
  - [12] T.M. O’Neil, *Phys. Fluids* **23**, 725 (1980).
  - [13] S.A. Prasad and T.M. O’Neil, *Phys. Fluids* **26**, 665 (1983); A.W. Trivelpiece and R.W. Gould, *J. Appl. Phys.* **30**, 1784 (1959).